RM No. A8J21



RESEARCH MEMORANDUM

WIND-TUNNEL INVESTIGATION OF HORIZONTAL TAILS.

IV - UNSWEPT PLAN FORM OF ASPECT RATIO 2

AND A TWO-DIMENSIONAL MODEL

By Jules B. Dods, Jr.

Ames Aeronautical Laboratoryument on LOAN FROM THE FILES OF Moffett Field, Calif.

NASA FILE COPY

Loan expires on last
date stamped on back cover.
PLEASE RETURN TO
REPORT DISTRIBUTION SECTION
LANGLEY RESEARCH CENTER

NATIONAL AERONAUTICS AND SPACE ADMINISTRATION at the state of the stat

Langley Field, Virginia

CLASSIFIED DOCUMENT

This document contains classified information affecting the National Defense of the United States within the meaning of the Espionage Act, USC 60:13 and 32. Its transmission or the revelation of its contents in any manner to an unauthorized person is prohibited by law, Information so classified may be imparted only to persons in the military and naval services of the United States, appropriate civilian officers and employees of the Federal Government who have a legitimate Interest therein, and to United States citizens of known loyalty and discretion who of necessity must be informed thereof.

NASA FILE COPY

NATIONAL ADVISORY COMMITTEE FOR AERONAUTICS
LANGLEY AERO LOAD EXPIRES ON LOST TORY
LANGLEY Footomer to the content of the cont

PLEASE RETURN TO

REPUREPORT DISTRIBUTION SECTION

LANGLEY RESEARCH CENTER SED

NATIONAL AERONAUTICS AND

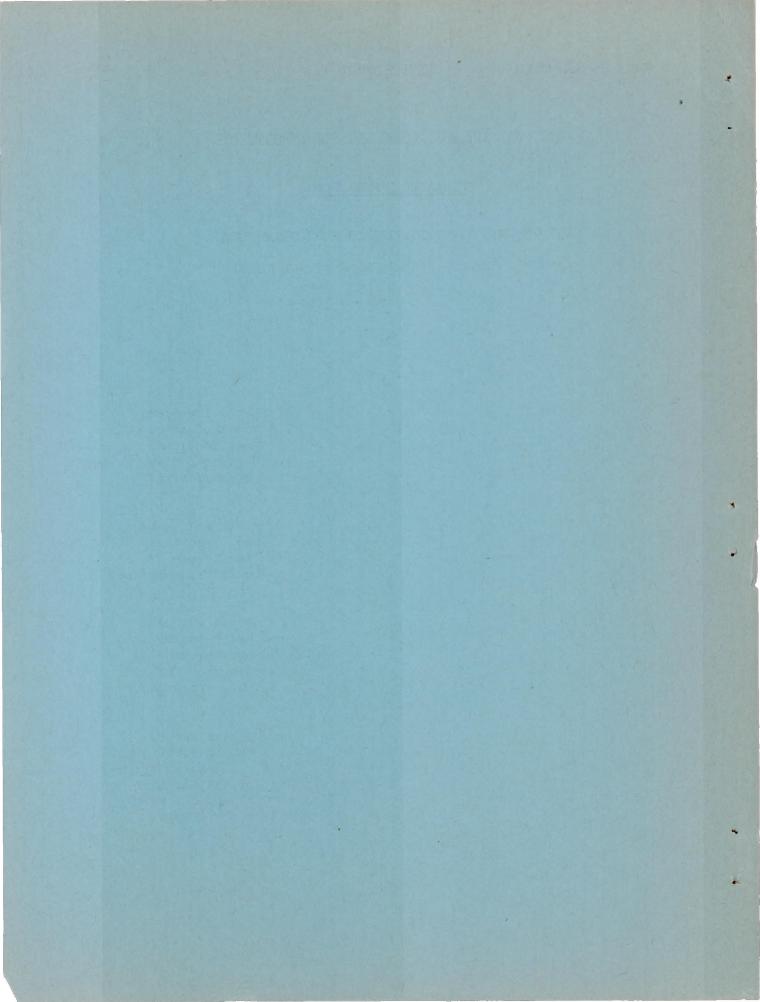
NATIO SPACE ADMINISTRATION FROMALTICS

1512 H STREE Langley Field, Virginia WASHINGTON 25, D. C.

NATIONAL ADVISORY COMMITTEE FOR AERONAUTICS

WASHINGTON December 16, 1948

RESTRICTED



NATIONAL ADVISORY COMMITTEE FOR AERONAUTICS

RESEARCH MEMORANDUM

WIND-TUNNEL INVESTIGATION OF HORIZONTAL TAILS.

IV - UNSWEPT PLAN FORM OF ASPECT RATIO

2 AND A TWO-DIMENSIONAL MODEL

By Jules B. Dods, Jr.

SUMMARY

The results of a wind-tunnel investigation of the low-speed aerodynamic characteristics of a horizontal-tail model of aspect ratio 2 having an "unswept" plan form, and of a two-dimensional model are presented. These data supplement previously reported results of tests on unswept and swept-back models of aspect ratios 3, 4.5, and 6.

The two-dimensional model, which has the same airfoil section as all the models tested in this series (NACA 64A010), provides data which can be used as the basis for computing the three-dimensional lift and hinge-moment parameters by the lifting-surface-theory procedure.

Test results are presented for the models with and without standard roughness applied to their leading edges, with sealed and unsealed radius—nose elevators, and for a Reynolds number ranging from 3.0 to $7.5 \times 10^{\circ}$. The tests included measurements of the model lift and pitching moment, elevator hinge moment, and pressure difference across the elevator nose seal.

The major effect of standard leading—edge roughness was to increase (positively) the rate of change of hinge—moment coefficient with angle of attack of the model of aspect ratio 2. Removal of the elevator nose seal reduced the lift effectiveness of the elevator for the two—dimensional model. No significant scale effects were encountered for either model through the Reynolds number range investigated.

INTRODUCTION

A systematic investigation of the control—surface characteris—tics, particularly the hinge—moment parameters, of horizontal—tail surfaces has been undertaken by the NACA to provide experimental results for a comparison with those parameters computed by lifting—surface—theory procedures.

Experimental results obtained from wind-tunnel tests of unswept and 35° swept-back plan-form models of aspect ratios 3, 4.5, and 6 are presented in references 1, 2, and 3. The present report extends the experimental data to include an aspect ratio of 2 and, in addition, presents section data which are necessary for the lifting-surface—theory computations. A comparison of the experimental and theoretical results for the unswept and the swept-back plan forms of aspect ratios 3 and 4.5 has been presented in reference 4.

COEFFICIENTS AND SYMBOLS

The coefficients and symbols used throughout the report are defined as follows:

Coefficients

c_{h_e}	elevator hinge-moment coefficient $(H/qS_e\overline{c}_e)$ (See appendix.)
che	section hinge-moment coefficient [h/q(ce;)2]
$C_{\mathbf{L}}$	lift coefficient (L/qS)
cl	section lift coefficient (1/qc)
$C_{\mathbf{m}}$	pitching-moment coefficient (M/qSc)
c _m	section pitching-moment coefficient $(m/q\overline{c}^2)$
Δp/q	pressure coefficient across elevator nose seal (pressure below seal minus pressure above seal divided by the free-stream dynamic pressure)

Symbols

Α .	aspect ratio (2b2/S)
Ъ	span of the model, feet
c	chord of the model, feet
c	mean aerodynamic chord $\left(\frac{\int_{0}^{b} c^{2}db}{\int_{0}^{b} c db}\right)$, feet
¯c _e	root-mean-square elevator chord aft of the hinge line measured parallel to the plane of symmetry, feet
ce t	chord of the elevator aft of the hinge line measured perpendicular to the hinge line, feet
н	hinge moment, foot-pounds
h	section hinge moment, foot-pounds
L	lift, pounds
1	section lift, pounds
М	pitching moment about a lateral axis through the 0.25 c point, foot-pounds
M _A	first moment of the elevator area aft of the hinge line about the hinge line, feet cubed
q	free-stream dynamic pressure $(\frac{1}{2}\rho V^2)$, pounds per square foot
R	Reynolds number (pVc/\(\mu\))
S	area of model, square feet
Se	area of the elevator aft of the hinge line, square feet
V	velocity of air, feet per second

- a corrected angle of attack, degrees
- αο corrected section angle of attack, degrees
- δ_e elevator deflection (positive when trailing edge of elevator is down) measured in a plane normal to the hinge line, degrees
- μ absolute viscosity, slugs per foot-second
- ρ density of air, slugs per cubic foot

Parameters

$$\alpha_{\delta_e} = -\frac{c_{L_{\delta_e}}}{c_{L_{\alpha}}}, \quad \text{or} \quad -\frac{c_{l_{\delta_e}}}{c_{l_{\alpha_o}}}$$
 elevator—effectiveness parameter

•
$$c_{h_{\alpha}} = \left(\frac{\partial c_{h_{e}}}{\partial \alpha}\right)_{\delta_{e}=0}$$
; $c_{h_{\alpha_{o}}} = \left(\frac{\partial c_{h_{e}}}{\partial \alpha_{o}}\right)_{\delta_{e}=0}$ (measured through $\alpha=0$ or $\alpha_{o}=0$)

$$c_{h_{\delta_e}} = \left(\frac{\delta c_{h_e}}{\delta \delta_e}\right)_{\alpha=0} \quad \text{; } c_{h_{\delta_e}} = \left(\frac{\delta c_{h_e}}{\delta \delta_e}\right)_{\alpha_o=0} \quad \text{(measured through } \delta_e=0\text{)}$$

$$C_{L_{\alpha}} = \left(\frac{\partial C_{L}}{\partial \alpha}\right)_{\delta_{e}=0}$$
; $c_{l_{\alpha_{o}}} = \left(\frac{\partial c_{l}}{\partial \alpha_{o}}\right)_{\delta_{e}=0}$ (measured through $\alpha=0$ or $\alpha_{o}=0$)

$$c_{L\delta_e} = \left(\frac{\partial c_L}{\partial \delta_e}\right)_{\alpha=0}$$
; $c_{l\delta_e} = \left(\frac{\partial c_l}{\partial \delta_e}\right)_{\alpha_0=0}$ (measured through $\delta_e=0$)

MODELS

The unswept horizontal tail model tested in this investigation had an aspect ratio of 2 and a taper ratio (ratio of tip chord to root chord) of 0.5. The 0.70-chord line (elevator hinge line) was perpendicular to the simulated plane of symmetry, resulting in a 16.7° angle of sweepback of the 0.25-chord line, as shown in figure 1.

The two-dimensional model had a chord of 3.5 feet, and spanned the 7-foot dimension of the 7- by 10-foot wind-tunnel test section.

Both models were equipped with a sealed radius—nose 0.30—chord elevator. The airfoil section which was parallel to the air stream was the same as for the models of references 1, 2, and 3. The slight discrepancies between the model coordinates and the true NACA 64A010 coordinates (table I) are not considered important.

The gaps between the elevators and the shrouds and the gaps between the elevator noses and the balance plates (seal gap) are shown in figure 1. The elevator nose gaps were sealed over the complete span of both models. In addition, the elevator of the two-dimensional model was sealed at either end and the elevator of the model of aspect ratio 2 was sealed at the inboard end and at the outboard hinge bracket (82-percent span). The inboard hinge bracket of the model of aspect ratio 2 and the two hinge brackets of the two-dimensional model were located outside of the air stream. Pressure orifices were located in the balance chambers enclosed by the shrouds both above and below the nose seal at several spanwise stations. The orifices at 91-percent span of the model of aspect ratio 2 were outboard of the hinge bracket.

The tip shape of the model of aspect ratio 2 was formed by rotating the tip airfoil section parallel to the undisturbed air stream about a line inboard of the tip, a distance equal to the maximum tip ordinate.

Photographs showing the models mounted in the wind tunnel are presented in figures 2 and 3.

TESTS

The tests were conducted in the Ames 7- by 10-foot wind tunnels. The model of aspect ratio 2 was mounted on a turntable flush with the floor (fig.2), and was tested with a dynamic pressure of 28 pounds

per square foot, corresponding to a Reynolds number of 3.0×10^6 . A limited amount of data was also obtained at Reynolds numbers of 5.0 and 7.5×10^6 . The two-dimensional model (fig. 3) was tested at dynamic pressures of 22.5, 40, 57, and 75.5 pounds per square foot¹, resulting in Reynolds numbers of 3.0, 4.0, 4.8, and 5.5×10^6 . All tests were conducted with the models in the smooth condition with the elevator sealed unless otherwise specified. For those tests with leading-edge roughness, standard roughness was applied as defined in reference 5.

Model lift and pitching moment were measured by means of the wind-tunnel balance system. Elevator hinge moments were measured by means of resistance—type torsional strain gages. Pressures above and below the elevator nose seal in the balance chamber were measured by the use of a manometer connected to the orifices in the elevator balance chamber.

CORRECTIONS

All coefficients and the angle of attack have been corrected for the effects of the tunnel walls by the methods of references 6 and 7. The corrections listed below were added to the data:

Aspect ratio 2 model	Two-dimensional model		
$\Delta \alpha_1 = 0.934 c_{\text{Lu}}$	$\Delta \alpha_{0_{1}} = 0.234 \mathbf{c}_{1\mathbf{u}}$		
$\Delta \alpha_2 = 0.174 \text{ CL}_{\text{u}}(\delta_{\text{e}}=0)$	$\Delta \alpha_{o2} = 0.937 c_{m_U}$		
$\Delta C_{m} = 0.00499 C_{L_{U}}$	$\Delta c_{\rm m} = 0.9907 c_{\rm m_u} + 0.00656 c_{lu}$		
$\Delta c_{h_e} = 0.00678 c_{L_u}$	$\Delta c_{h_e} = 0.00846 c_{l_u}$		
$C_{L} = 0.993 C_{L_{11}}$	$c_l = 0.965 c_{l_{11}}$		

where

 $\Delta\alpha_1$, $\Delta\alpha_{01}$ jet-boundary correction to angle of attack $\Delta\alpha_2$, $\Delta\alpha_{02}$ streamline-curvature correction to angle of attack

¹The values of the dynamic pressure of 40, 57, and 75.5 pounds per square foot are the test dynamic pressures corresponding to a Reynolds number of 3.0×10^6 for the models of references 1, 2, and 3.

△Cm, △cm correction to pitching-moment coefficient

ΔChe, Δche correction to hinge-moment coefficient

CL, cl, uncorrected lift coefficient

cmu uncorrected section pitching-moment coefficient

RESULTS AND DISCUSSION

The results of tests of the model of aspect ratio 2 are presented in figures 4 to 9 and those for the two-dimensional model are presented in figures 10 to 18.

The variations of lift, hinge-moment, and pitching-moment coefficients with angle of attack are given in figure 4 for the model of aspect ratio 2 and in figure 10 for the two-dimensional model at a Reynolds number of 3.0 × 10°. Hinge-moment coefficients are also shown as a function of the elevator angle for various angles of attack in figures 5 and 11. Additional data obtained for the two-dimensional model at Reynolds numbers of 4.0, 4.8, and 5.5 × 10° are presented in figures 12, 13, and 14. The variation of the pressure coefficient across the elevator nose seal with angle of attack is presented in figures 6 and 15. The effects of variations of the Reynolds number, standard leading-edge roughness, and removal of the elevator nose seal on the lift and hinge-moment coefficients are shown in figures 7 to 9 for the model of aspect ratio 2 and in figures 16 to 18 for the two-dimensional model.

Effectiveness and Hinge-Moment Parameters

The lift-effectiveness and the hinge-moment parameters are listed in table II². As shown in the table, $C_{h_{\alpha}}$ for the model of aspect ratio 2 was -0.0002, and the section $c_{h_{\alpha_0}}$ was -0.0057; the value of $C_{h\delta_e}$ (-0.0072) for the model of aspect ratio 2 was likewise lower than the corresponding section $c_{h\delta_e}$ (-0.0114). The elevator-effectiveness parameter α_{δ_e} was higher for the model of

The parameters for the two-dimensional model are presented for R, 4.0×10^6 in table II. These values are essentially the same as those obtained at R, 3.0×10^6 for the model in the smooth condition with the elevator sealed.

aspect ratio 2 (-0.73) than for the two-dimensional model (-0.60) primarily because of the low lift-curve slope ($C_{L_{CL}} = 0.040$) associated with the low-aspect-ratio plan form.

Static Longitudinal Stability

The variation of pitching-moment coefficient with angle of attack (fig. 4(c)) indicates that the model of aspect ratio 2 was statically unstable $[(dC_m/d\alpha)_{\delta_e=0}=0.0023]$, measured through zero angle of attack, but that the static longitudinal stability increased at the stall, as would be predicted from the results of reference 8. The two-dimensional model was marginally unstable $[(dc_m/d\alpha_o)_{\delta_e=0}=0.0004]$ as shown in figure 10(c). No data were obtained for the two-dimensional model beyond the stall because the model was not designed to withstand the severe buffeting which occurred at the stall.

Scale Effect

The effects of variations of the Reynolds number are shown in figure 7 for the model of aspect ratio 2 and in figure 16 for the two-dimensional model. Data for he model of aspect ratio 2 were obtained for a Reynolds number range from 3.0 to 7.5×10^6 , and the range for the two-dimensional model was from 3.0 to 5.5×10^6 .

The maximum lift coefficient of the model of aspect ratio 2 increased slightly with increasing Reynolds number, but there was no change in the lift or hinge-moment parameters (measured through zero angle of attack).

A small increase in the lift-curve slope ($\Delta c_{l_{\alpha_O}} = 0.002$) was measured for the two-dimensional model at the highest Reynolds number. The rate of change of hinge-moment coefficient with angle of attack $c_{h_{\alpha_O}}$ was constant over the Reynolds number range, but there was a small irregular variation in the rate of change of hinge-moment coefficient with elevator deflection $c_{h_{\alpha_O}}$.

Effect of Standard Roughness

The effects of standard leading-edge roughness upon the lift and hinge-moment coefficients are shown in figure 8 for the model of aspect ratio 2 and in figure 17 for the two-dimensional model.

NACA RM No. A8J21

Normally, the effect of standard roughness is to increase the lift coefficient by an increase in the angle of stall. However, the angle of stall for the model of aspect ratio 2 was initially so large (low-aspect-ratio effect) that standard roughness was practically ineffective in increasing the angle of stall beyond that of the model in the smooth condition. For this reason, only nominal increases in the maximum lift coefficient were obtained.

The value of $C_{h\alpha}$ was changed from -0.0002 to 0.0006 by roughness, and $C_{h\delta_e}$ was changed from -0.0072 to -0.0070. The elevator-effectiveness parameter α_{δ_e} was unchanged.

Standard roughness on the two-dimensional model had no appreciable effect on any parameter except $c_{h\delta_e}$, which was changed from -0.011 l_1 to -0.0108 3 . The effects on the maximum lift coefficient were not measured.

Effect of Removing Elevator Nose Seal

The major effect of removing the elevator nose seal (models in smooth condition) was to reduce the lift-effectiveness parameter cl_{δ_e} of the two-dimensional model. As shown in table II, cl_{δ_e} was reduced from 0.065 to 0.063 for the two-dimensional model, but was unchanged for the model of aspect ratio 2. The lift-curve slope was unchanged for the model of aspect ratio 2, but the maximum lift coefficient was reduced. (See fig. 9(a).) The lift-curve slope of the two-dimensional model was reduced from 0.108 to 0.104. Hinge-moment parameters (measured through zero angle of attack and zero elevator deflection) were relatively unaffected by removal of the seal for either model. However, for large elevator deflections the hinge moments were somewhat increased, as shown in figures 9(b) and 18(b).

CONCLUSIONS

The results of tests conducted to evaluate the low-speed aerodynamic characteristics of an unswept horizontal tail model of aspect ratio 2 and a two-dimensional model having the same airfoil section indicate that:

The values of the lift and hinge-moment parameters presented in table II were derived from large-scale plots of the data.

- 1. No significant scale effects were encountered for either model for Reynolds numbers from 3.0 to 5.5×10^6 .
- 2. The effect of standard leading-edge roughness on the model of aspect ratio 2 was to change $C_{h_{\alpha}}$ from -0.0002 to 0.0006. The elevator-effectiveness parameter $\alpha_{\delta_{e}}$ was unchanged.
- 3. Removal of the elevator nose seal reduced the lift-effectiveness parameter $c_{l\delta_e}$ from 0.065 to 0.063 for the two-dimensional model.

Ames Aeronautical Laboratory,
National Advisory Committee for Aeronautics,
Moffett Field, Calif.

APPENDIX

Conversion Factors for Hinge-Moment Coefficients

Because several methods are in use for the conversion of hinge moments to nondimensional coefficient form, factors relating the various methods are presented. To obtain the hinge-moment coefficients for one of the listed methods, multiply the value of the hinge-moment coefficients of this report by the corresponding factor in the following table:

	Aspect r	atio 2 model
Equations for hinge-moment coefficients	H qChe (ft3)	Conversion factor
$C_{h_e} = \frac{H}{qS_e\overline{c}_e}$	2.935	1.000
$C_{h_e} = \frac{H}{qb(\overline{c}_e)^2}$	2.987	.983
$c_{h_e} = \frac{H}{2qM_A}$	2.987	.983

Note: The factor for the two-dimensional model is unity for all the equations.

REFERENCES

- 1. Dods, Jules B., Jr.: Wind-Tunnel Investigation of Horizontal Tails. I Unswept and 35° Swept-Back Plan Forms of Aspect Ratio 3. NACA RM No. A7K24, 1948.
- 2. Dods, Jules B., Jr.: Wind-Tunnel Investigation of Horizontal Tails. II Unswept and 35° Swept-Back Plan Forms of Aspect Ratio 4.5. NACA RM No. A8Bll, 1948.
- 3. Dods, Jules B., Jr.: Wind-Tunnel Investigation of Horizontal Tails. III Unswept and 35° Swept-Back Plan Forms of Aspect Ratio 6. NACA RM No. A8H30, 1948.
- 4. Jones, Arthur L., and Sluder, Loma: An Application of Falkner's Surface—Loading Method to Predictions of Hinge—Moment Parameters for Swept—Back Wings. NACA TN No. 1506, 1948.
- 5. Abbott, Ira H., von Doenhoff, Albert E., and Stivers, Louis S., Jr.: Summary of Airfoil Data. NACA ACR No. L5CO5, 1945.
- 6. Swanson, Robert S., and Toll, Thomas A.: Jet-Boundary Corrections for Reflection-Plane Models in Rectangular Wind Tunnels. NACA Rep. No. 770, 1943.
- 7. Allen, H. Julian, and Vincenti, Walter G.: Wall Interference in a Two-Dimensional-Flow Wind Tunnel With Consideration of the Effect of Compressibility. NACA Rep. No. 782, 1944.
- 8. Shortal, Joseph A., and Maggin, Bernard: Effect of Sweepback and Aspect Ratio on Longitudinal Stability Characteristics of Wings at Low Speeds. NACA TN No. 1093, 1946.

TABLE I.— COORDINATES FOR THE NACA 64A010 AIRFOIL AND THE MODELS TESTED

[All Dimensions in Percent of Wing Chord]

Upper and Lower Surfaces				
Station	NACA 64A010 ordinate	Model ordinate		
0 .50 .75 1.25 2.50 5.00 7.50 10.00 15.00 20.00 25.00 30.00 35.00 40.00 45.00 50.00 60.00 65.00 70.00 75.00 80.00 90.00 95.00	0 .804 .969 1.225 1.688 2.327 2.805 3.199 3.813 4.272 4.606 4.837 4.968 4.995 4.894 4.684 4.388 4.021 3.597 3.127 2.623 2.103 1.582 1.062 541	0 .819 .987 1.247 1.696 2.333 2.780 3.202 3.816 4.280 4.610 4.842 4.950 4.975 4.889 4.672 4.373 4.011 3.594 3.131 2.637 2.120 1.595 1.071 .553 0		
L.E. radius 0.687 ^a T.E. radius 0.023 ^a				

^aSame for both the NACA 64A010 section and the models.

TABLE II.— A SUMMARY OF THE LIFT AND HINGE-MOMENT PARAMETERS OF THE UNSWEPT MODEL OF ASPECT RATIO 2 AND THE TWO-DIMENSIONAL MODEL

1				
100	A GENERAL	Model Condition		
Parameter	Model smooth; elevator sealed	Model with standard roughness; elevator sealed	Model smooth; elevator seal removed	
Aspect ratio 2; R, 3.0 × 10 ⁶				
$c_{h_{\alpha}}$	-0.0002	0.0006	-0.0002	
Ch8e	0072	0070	0074	
$c_{L^{\alpha}}$.040	.040	.040	
$c_{L_{\delta_e}}$.029	.029	.029	
^α δe	73	 73	73	
Two-dimensional; R, 4.0 × 10 6				
$c_{h\alpha_{o}}$	-0.0057	-0.0057	-0.0057	
c _h ₈ e	0114	0108	0112	
clao	.108	.108	.104	
clδe	.065	.065	.063	
αδе	60	60	60	



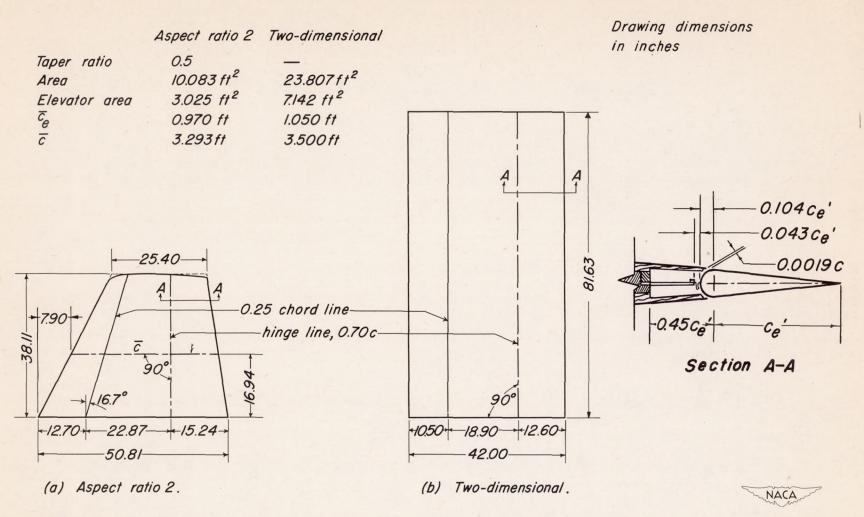
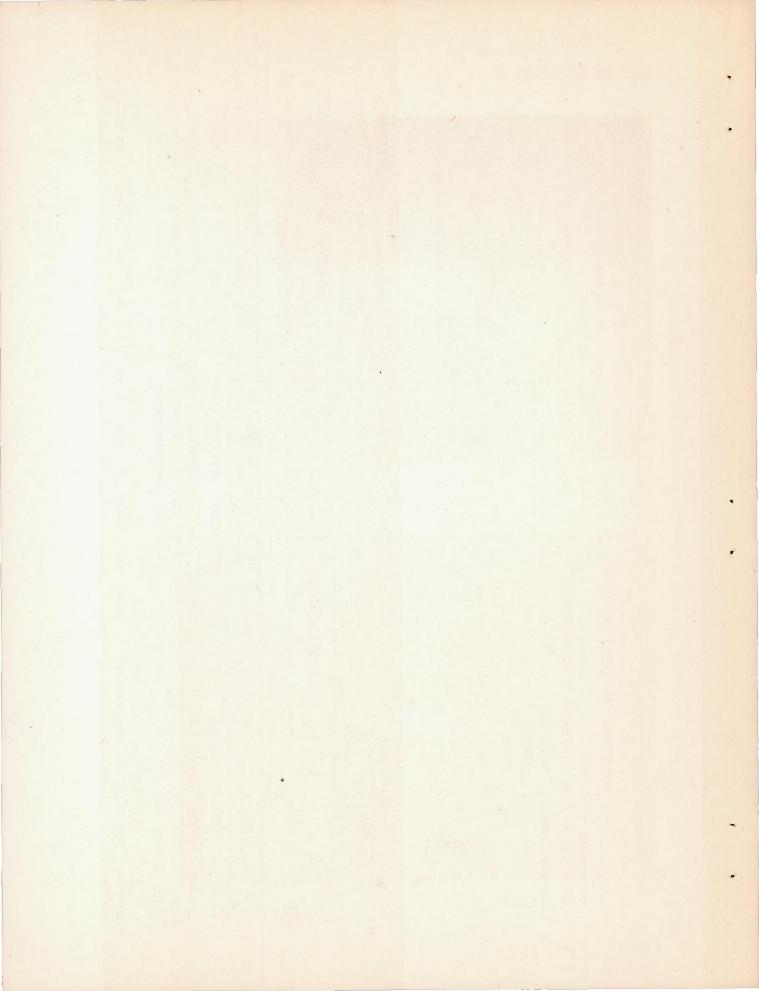
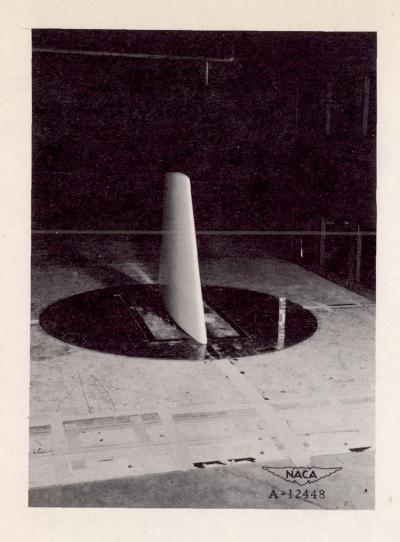
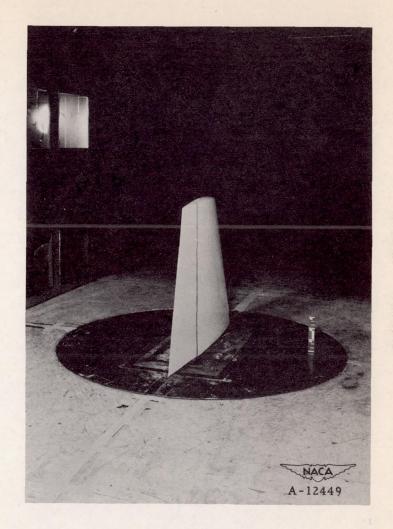


Figure I.- Plan forms of the unswept horizontal tail model of aspect ratio 2 and the two-dimensional model.



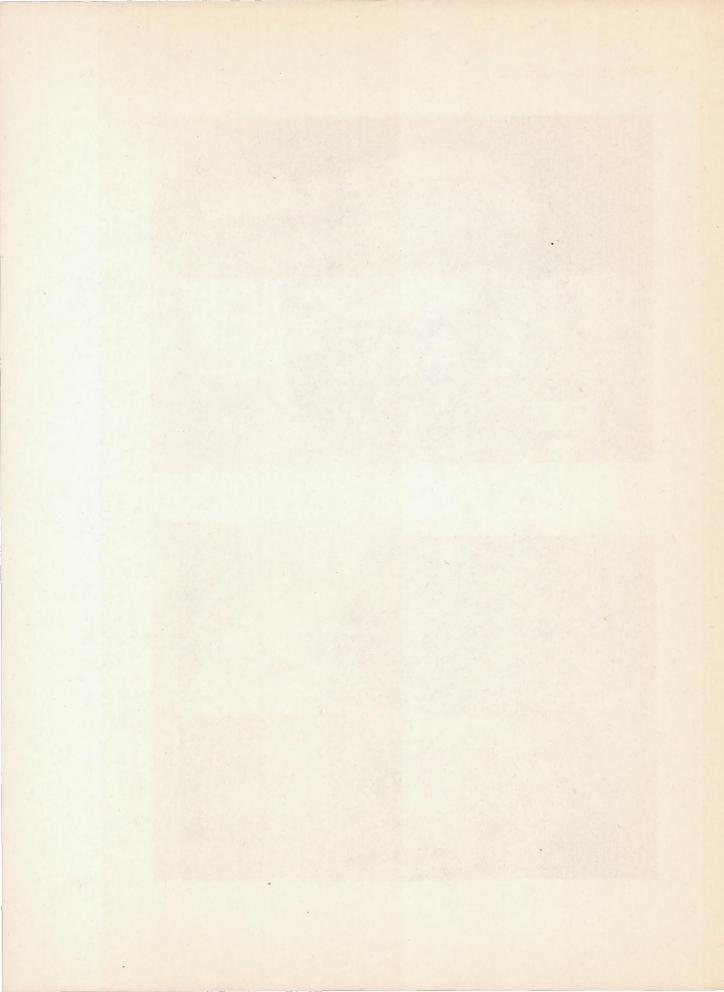




(a) Three-quarter front view.

(b) Three-quarter rear view.

Figure 2.- The model of aspect ratio 2 mounted in the 7- by 10-foot wind tunnel.

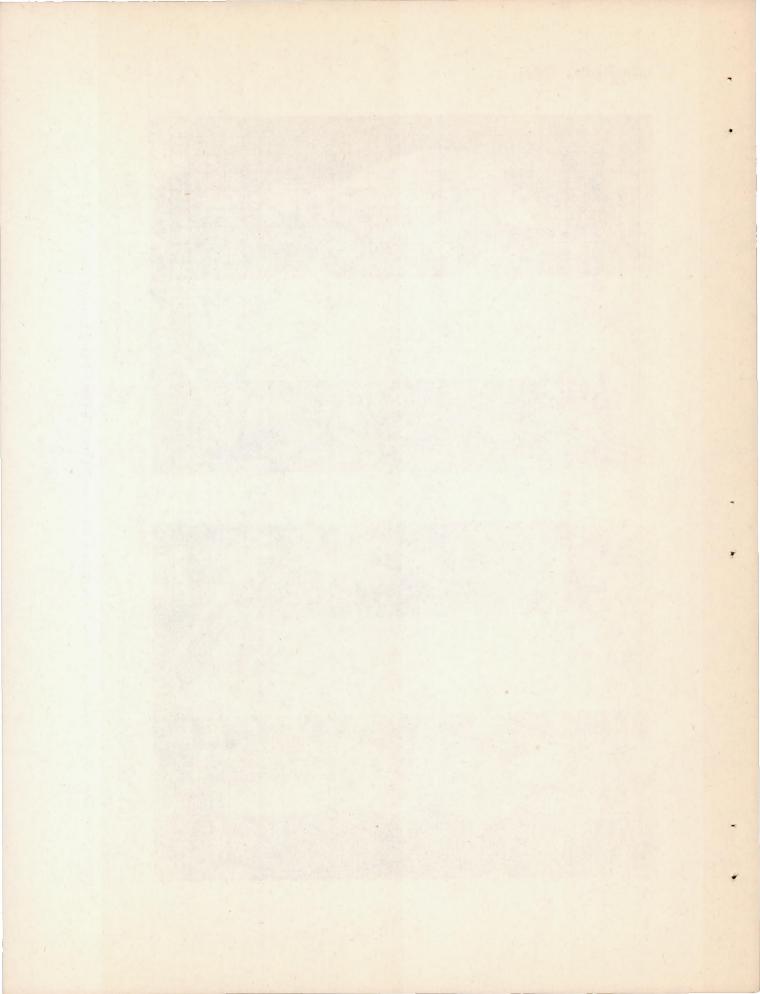




(a) Three-quarter front view.

(b) Three-quarter rear view.

Figure 3.- The two-dimensional model mounted in the 7- by 10-foot wind tunnel.



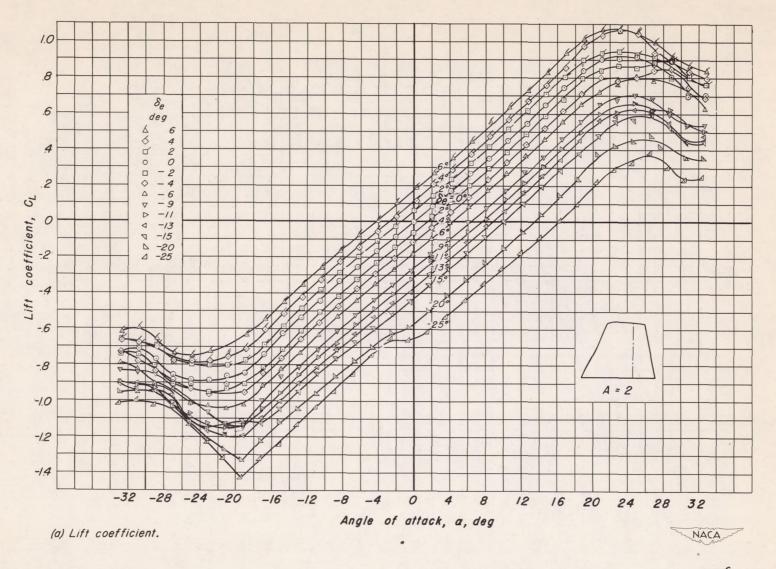
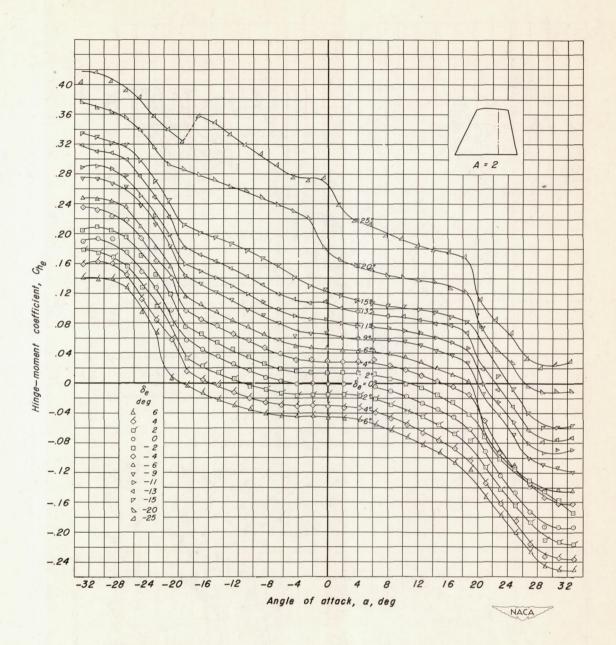


Figure 4.- Lift, hinge-moment, and pitching-moment coefficients for the model of aspect ratio 2. R, 3.0×10^6 .



(b) Hinge-moment coefficient.

Figure 4.- Continued.

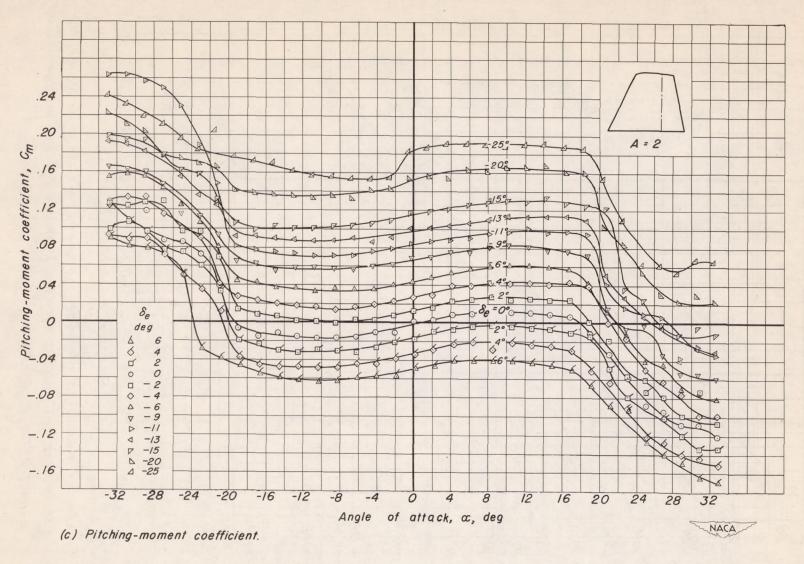


Figure 4.- Concluded.

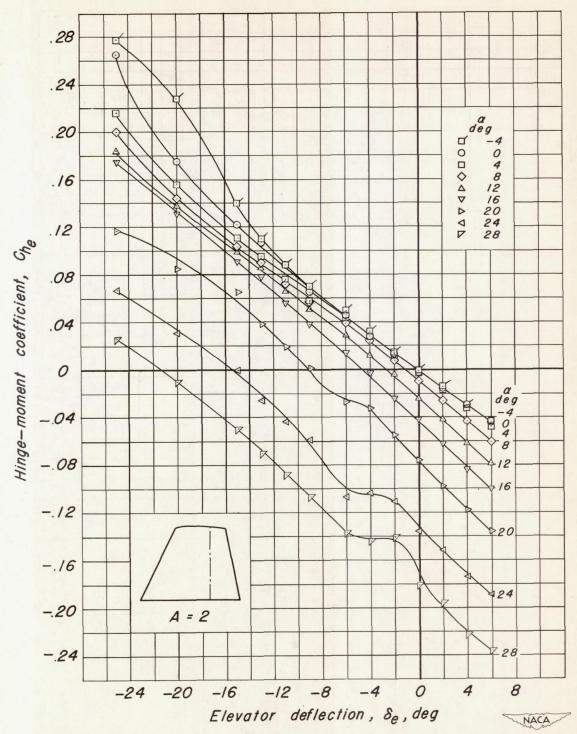
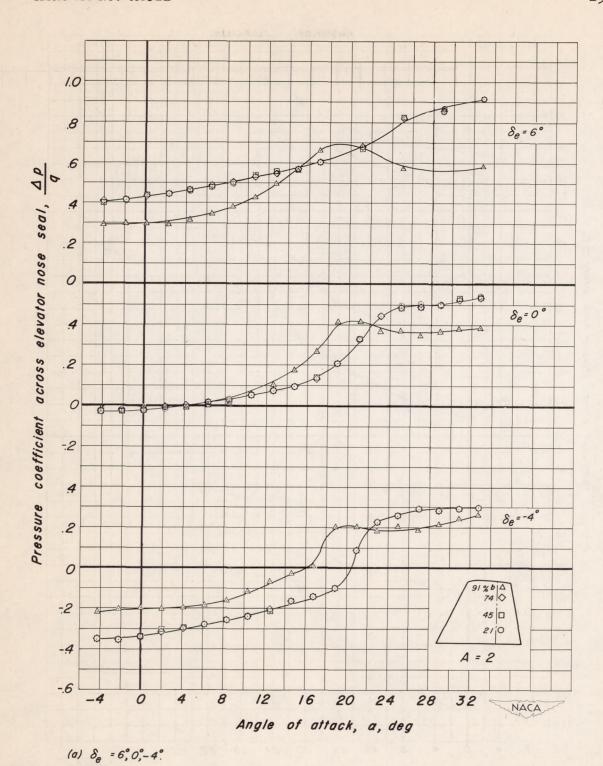


Figure 5.— Variation of hinge-moment coefficient with elevator deflection for various angles of attack for the model of aspect ratio 2. R, 3.0×10^6 .



Service Constitution

Figure 6.— Variation of pressure coefficient across elevator nose seal with angle of attack for the model of aspect ratio 2. R, 3.0×10^6 .

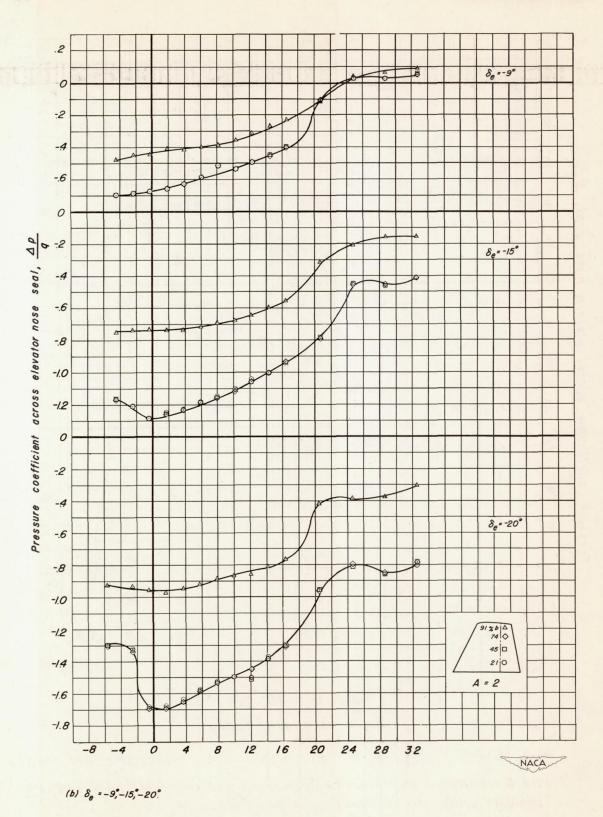
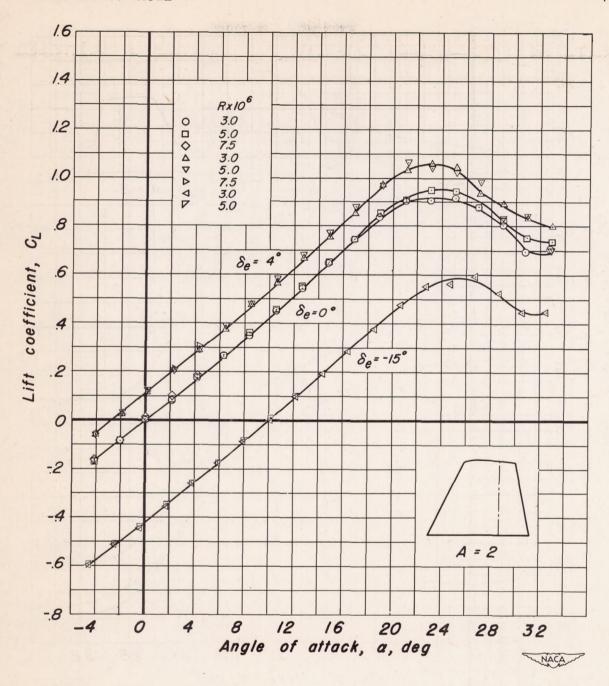


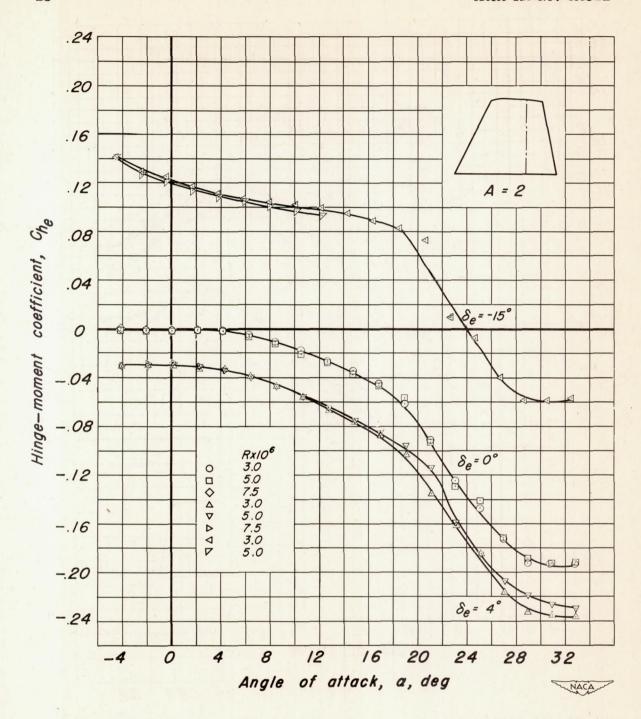
Figure 6.- Concluded.



· 国际中国的第一个一个中国的中国的

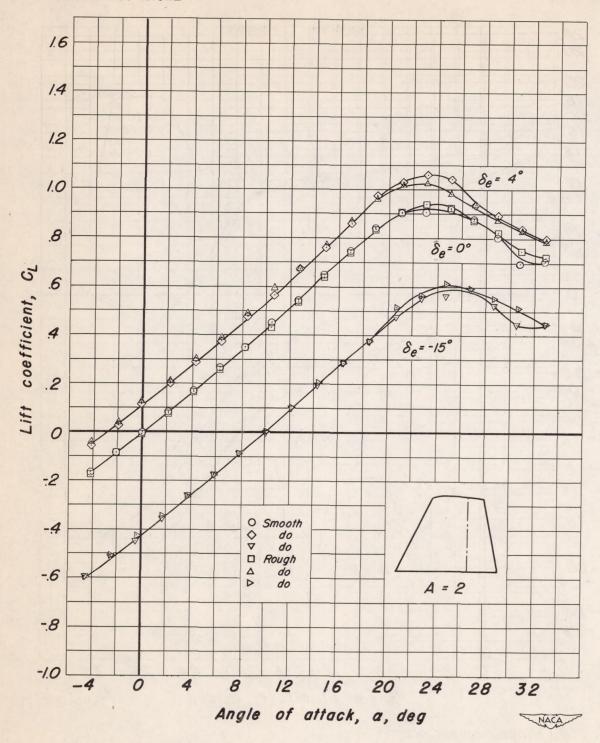
(a) Lift coefficient.

Figure 7.— Comparison of the lift and hinge-moment coefficients for various values of the Reynolds number for the model of aspect ratio 2.



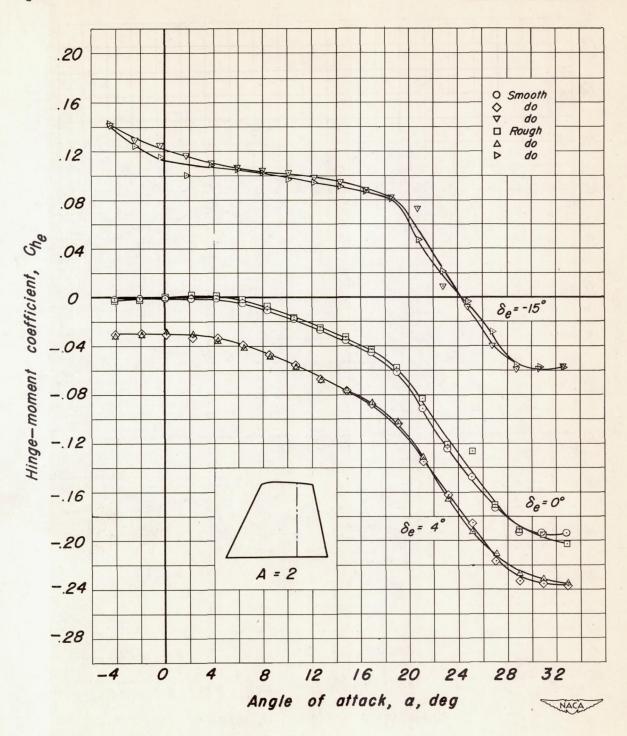
(b) Hinge-moment coefficient.

Figure 7.- Concluded.



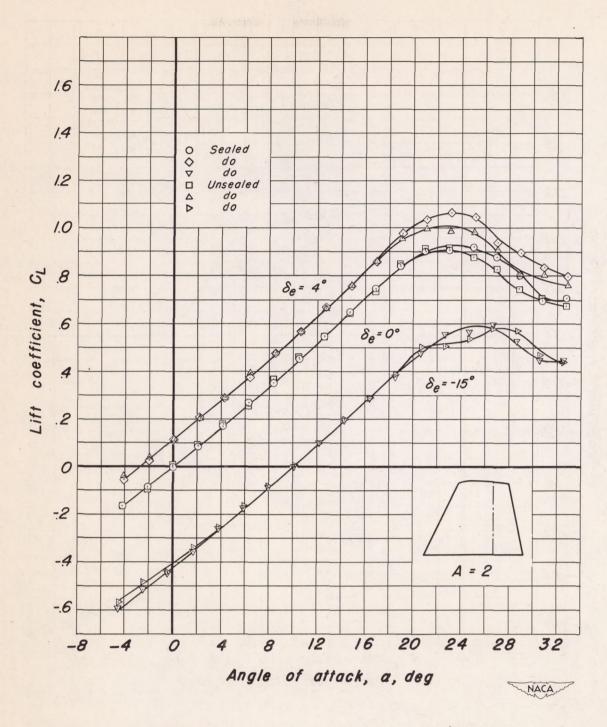
(a) Lift coefficient.

Figure 8.— Comparison of the lift and hinge-moment coefficients for the model of aspect ratio 2 with and without leading-edge roughness, R, 3.0 x 106.



(b) Hinge-moment coefficient.

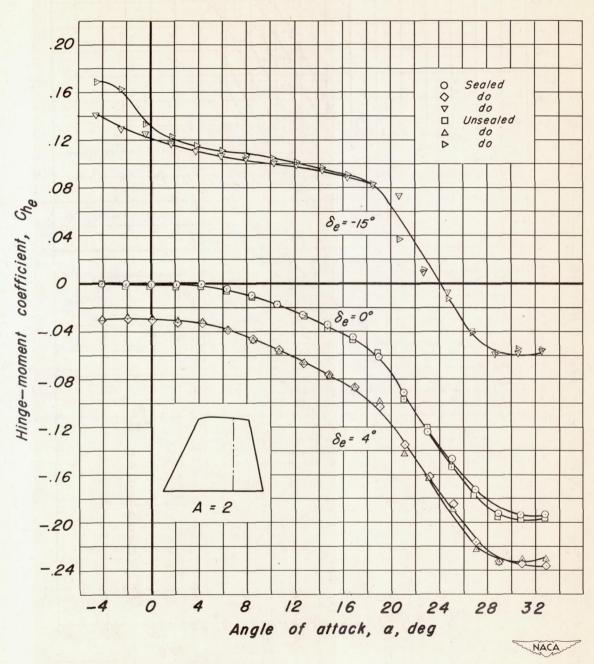
Figure 8.- Concluded.



September 1 to the september 1

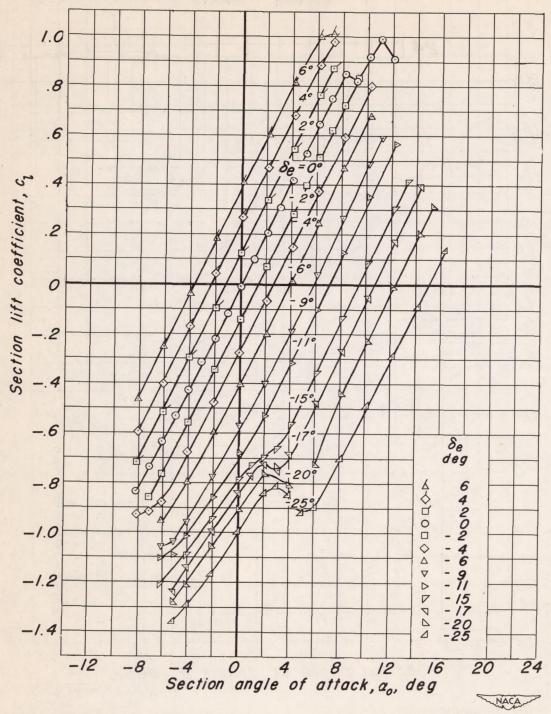
(a) Lift coefficient.

Figure 9.- Comparison of the lift and hinge-moment coefficients for the model of aspect ratio 2, with and without elevator seal. R, 3.0 x 10⁶.



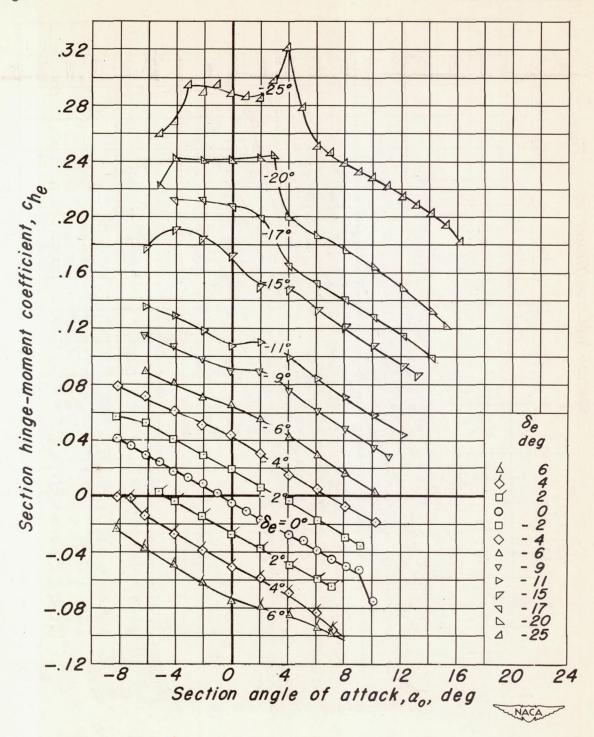
(b) Hinge-moment coefficient.

Figure 9.- Concluded.



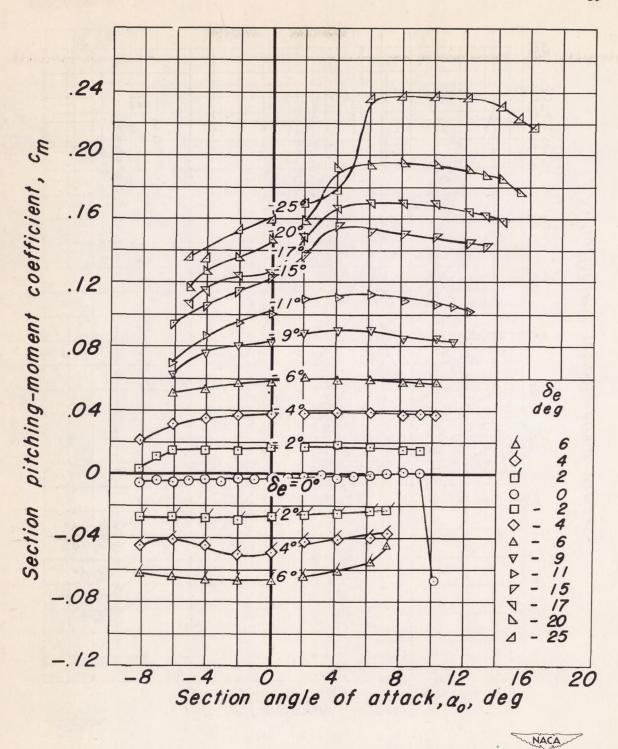
(a) Lift coefficient.

Figure 10. - Section lift, hinge-moment, and pitching-moment coefficients of the NACA 64A010 airfoil. R,3.0 x 10⁶.



(b) Hinge-moment coefficient.

Figure 10.-Continued.



(c) Pitching-moment coefficient.

Figure 10.—Concluded.

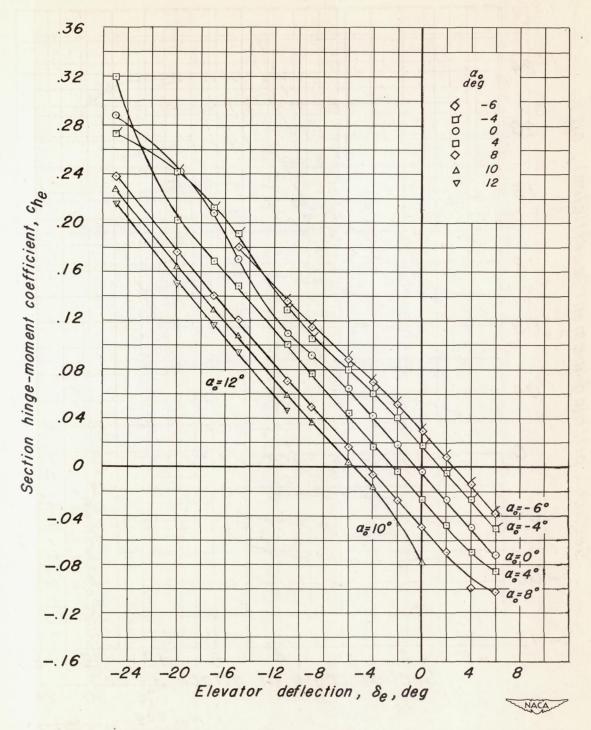
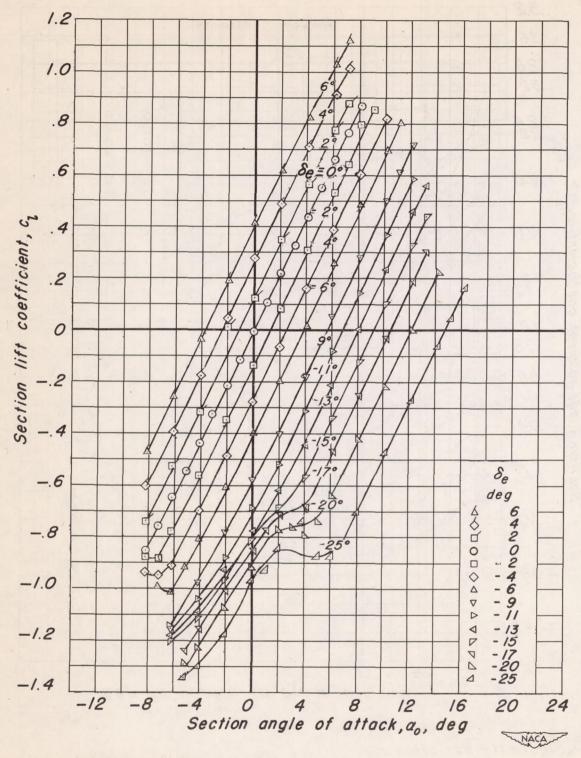
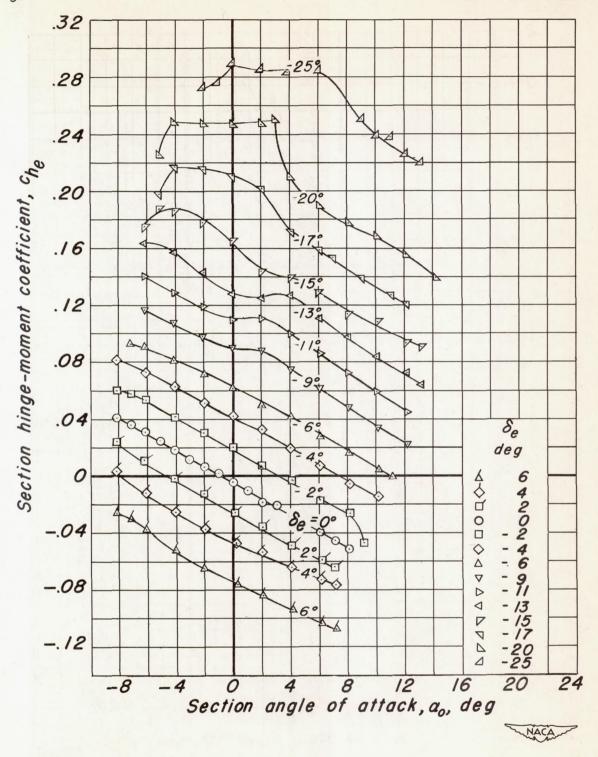


Figure II.— Variation of section hinge-moment coefficient with elevator deflection for various angles of attack of the NACA 64A0IO airfoil. R, 3.0x10⁶.



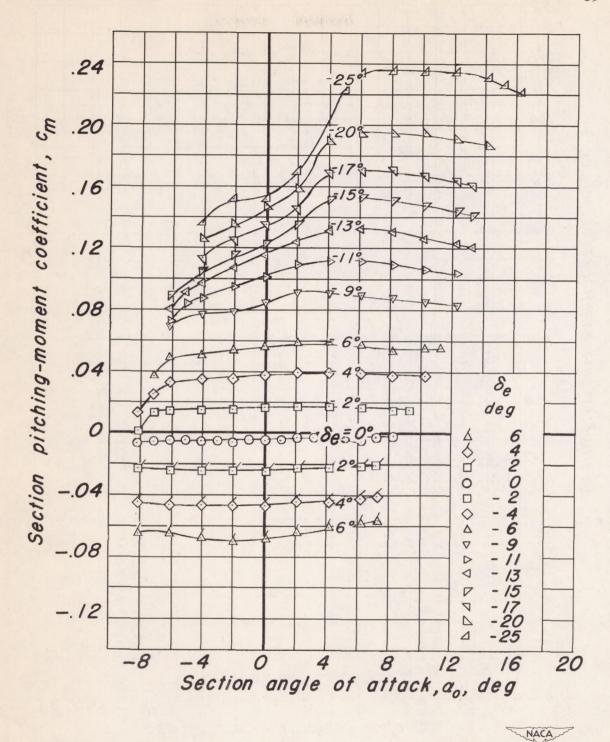
(a) Lift coefficient.

Figure 12.- Section lift, hinge-moment, and pitching-moment coefficients of the NACA 64A010 airfoil. R, 4.0 x 10⁶.



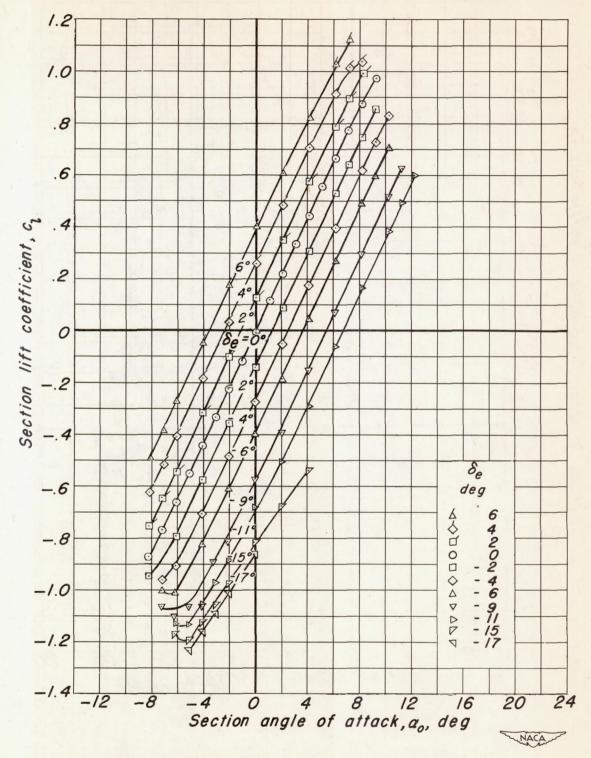
(b) Hinge-moment coefficient.

Figure 12.- Continued.



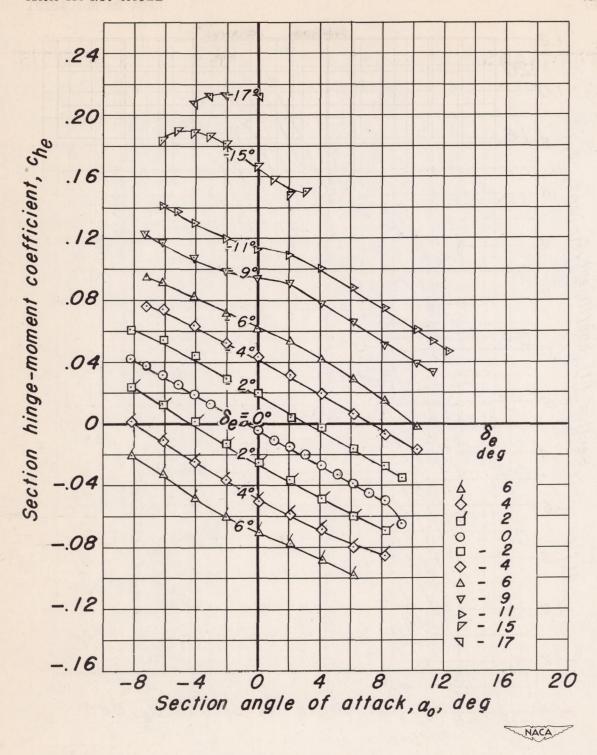
(c) Pitching-moment coefficient.

Figure 12.- Concluded.



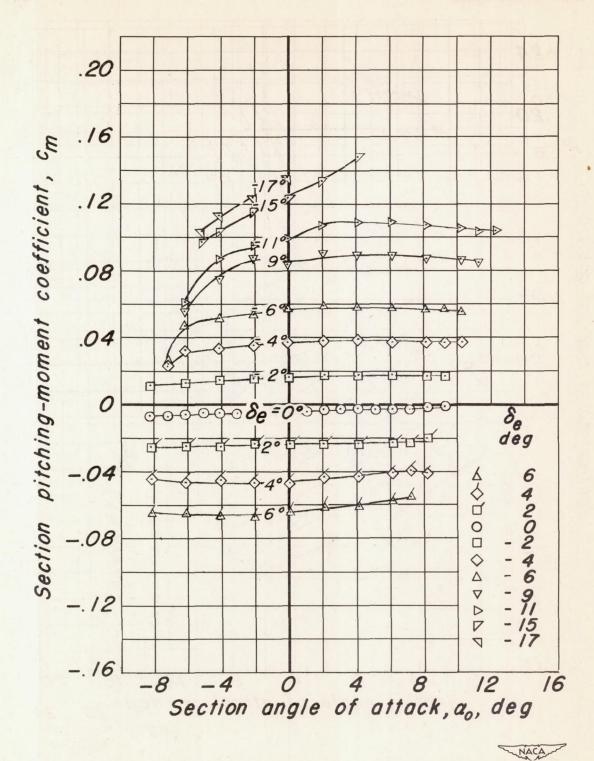
(a) Lift coefficient.

Figure 13.— Section lift, hinge-moment, and pitching-moment coefficients of the NACA 64AOIO airfoil. R, 4.8 x 106.



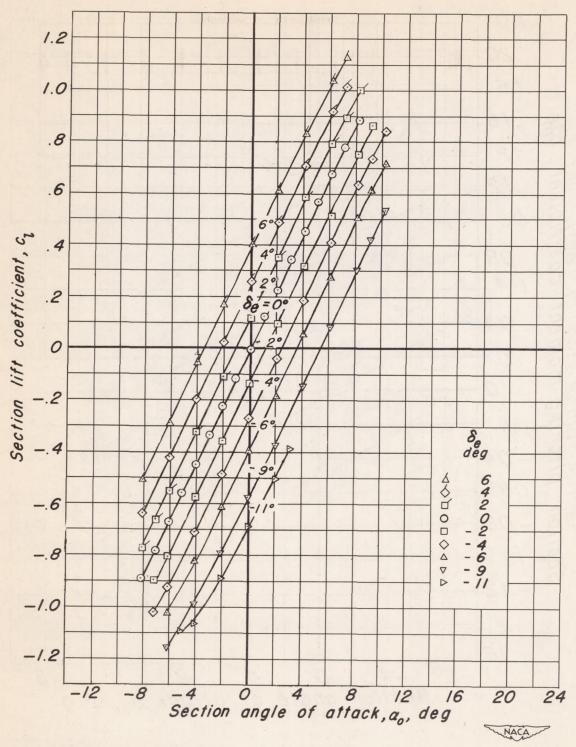
(b) Hinge-moment coefficient.

Figure 13.- Continued.



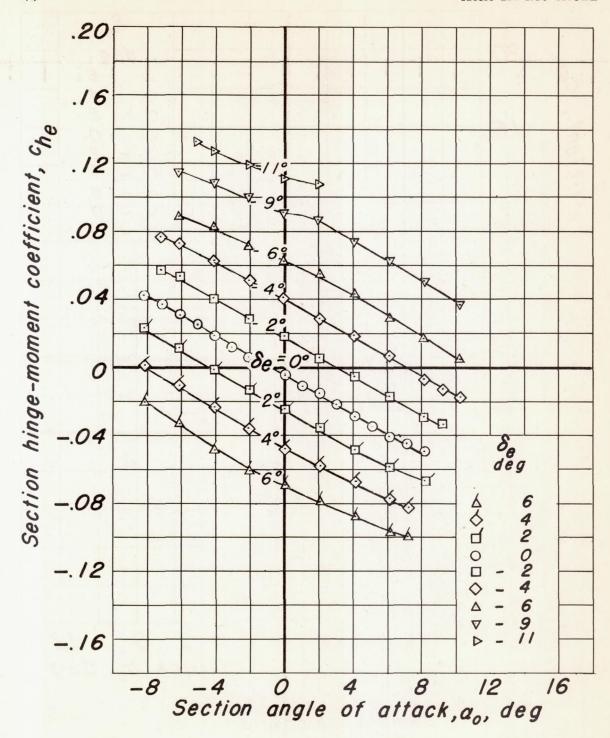
(c) Pitching-moment coefficient.

Figure 13.—Concluded.



(a) Lift coefficient.

Figure 14. - Section lift, hinge-moment, and pitching-moment coefficients of the NACA 64A010 airfoil. R, 5.5 x 10 6.

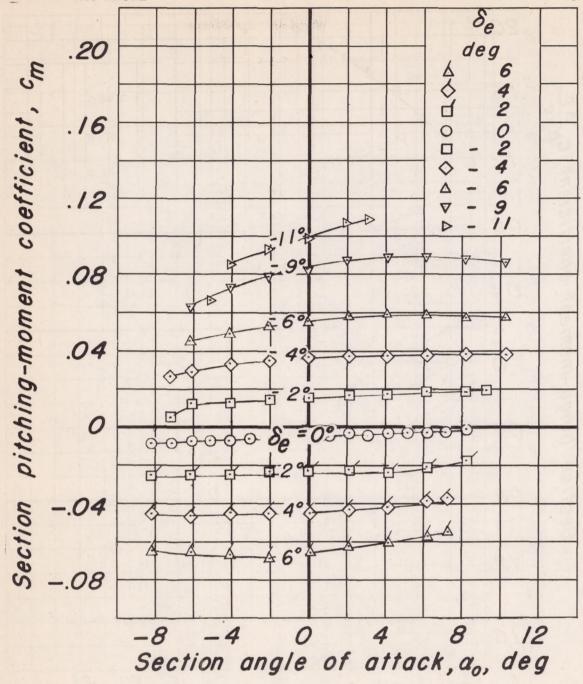


(b) Hinge-moment coefficient.

ent coefficient.

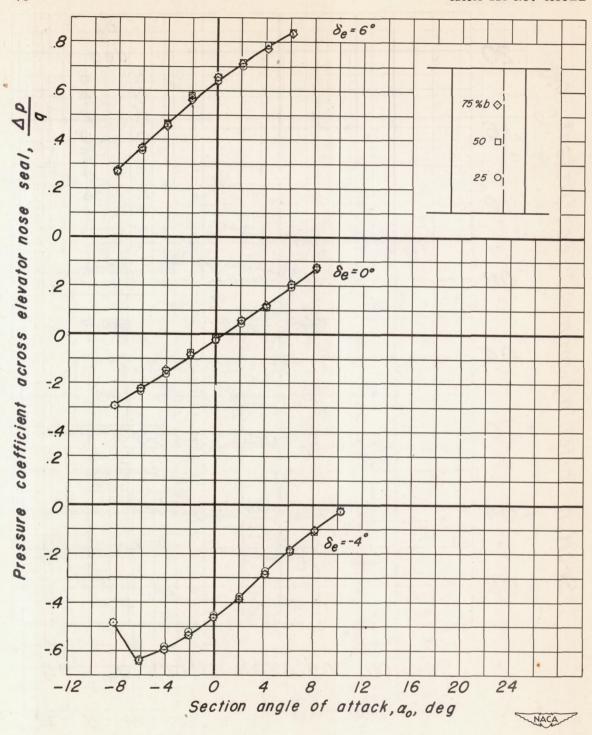
Figure 14.- Continued.

NACA



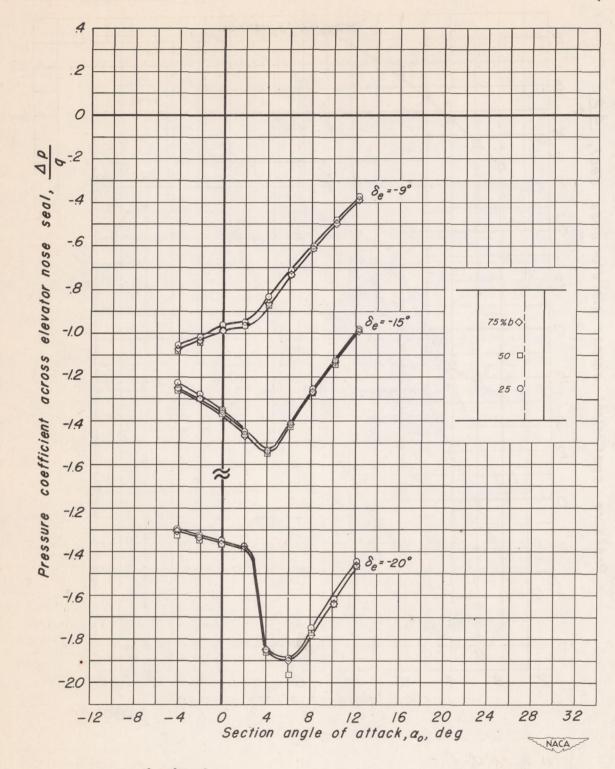
(c) Pitching-moment coefficient.

Figure 14.- Concluded.



(a) $\delta_{\theta} = 6,0,-4$.

Figure 15.- Variation of pressure coefficient across elevator nose seal with angle of attack of the NACA 64A010 airfoil R, 4.0 x 10⁶.



(b) $\delta_e = -9, -15, -20$.

Figure 15.- Concluded.

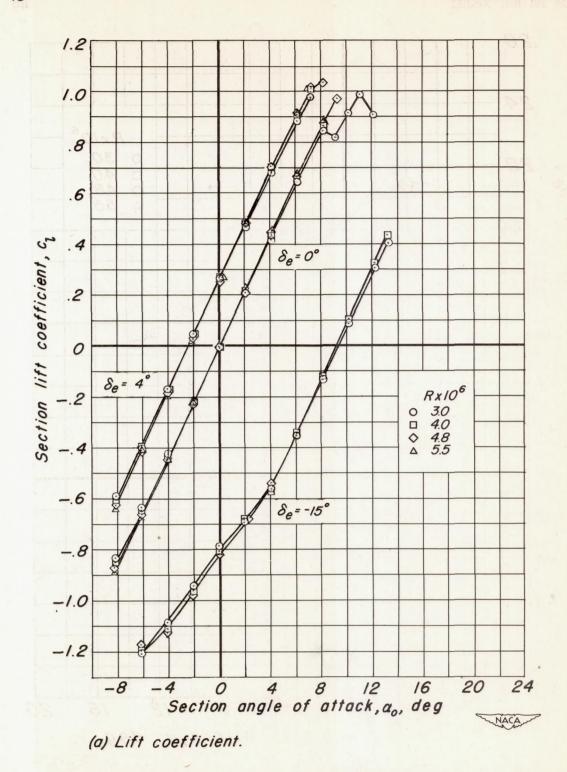
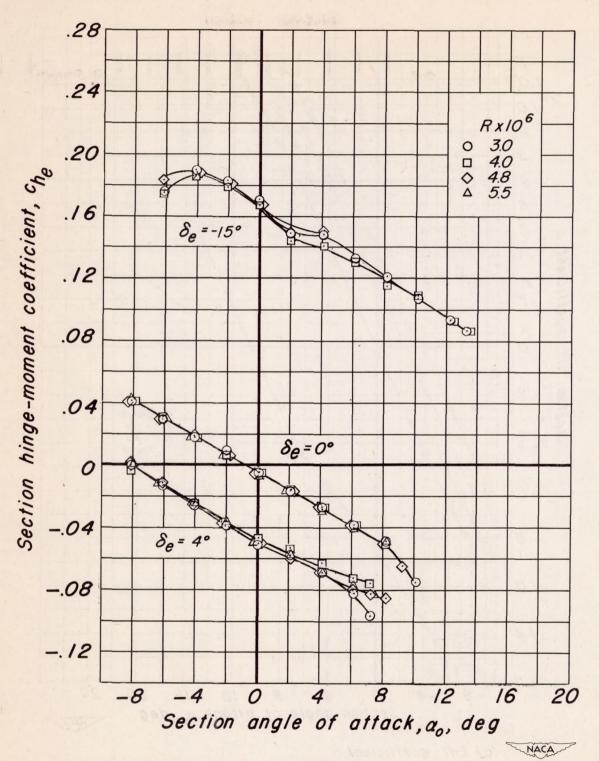
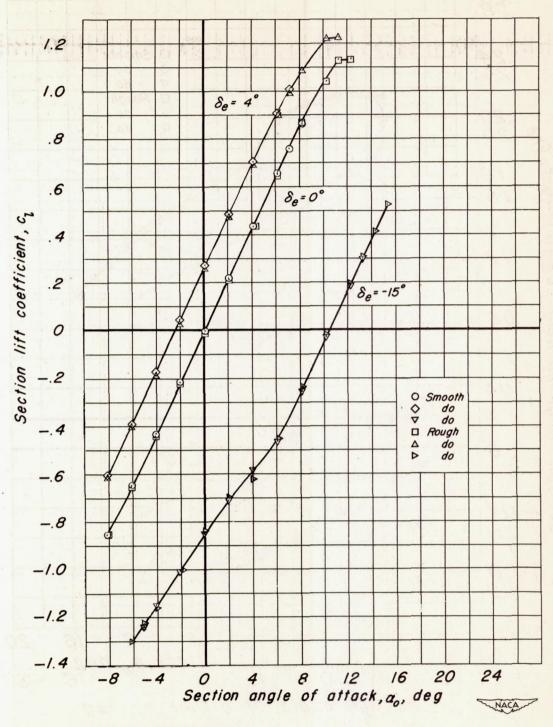


Figure 16.— Comparison of the section lift and hinge-moment coefficients of the NACA 64A010 airfoil at various Reynolds numbers.



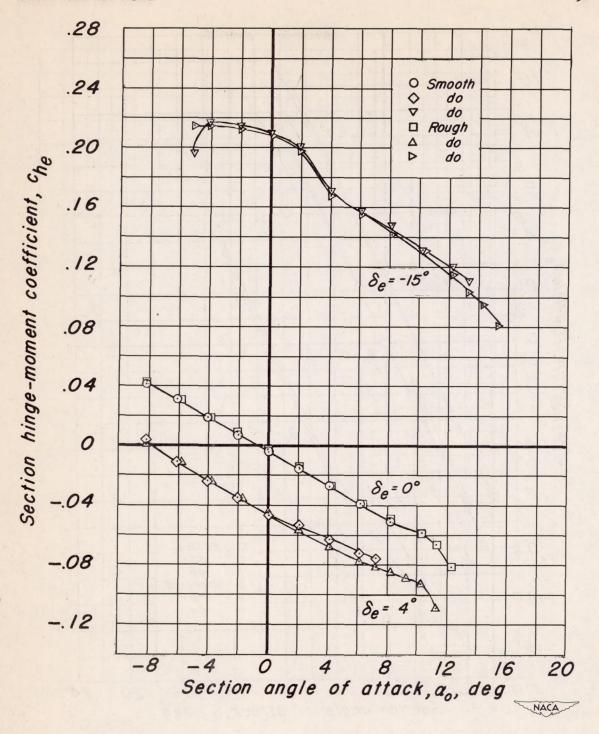
(b) Hinge-moment coefficient.

Figure 16.—Concluded.



(a) Lift coefficient.

Figure 17.- Comparison of the section lift and hinge-moment coefficients of the NACA 64A010 airfoil with and without leading-edge roughness. R, 4.0-x10⁶.



(b) Hinge-moment coefficient.

Figure 17.- Concluded.

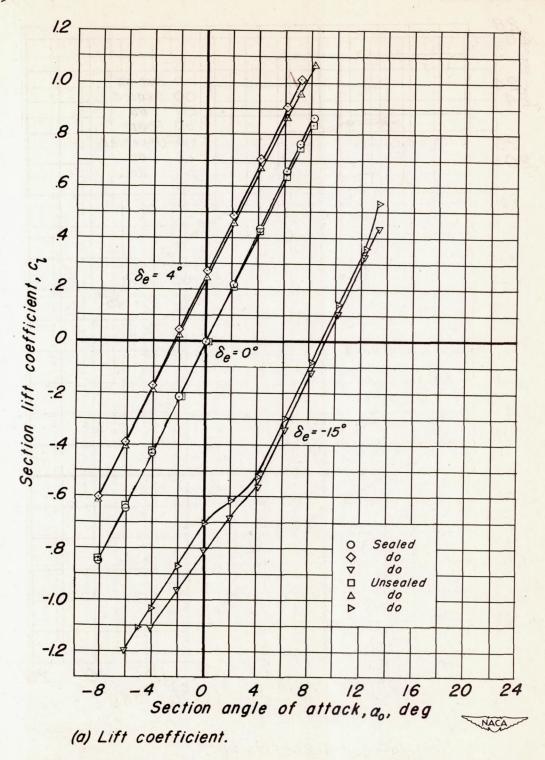
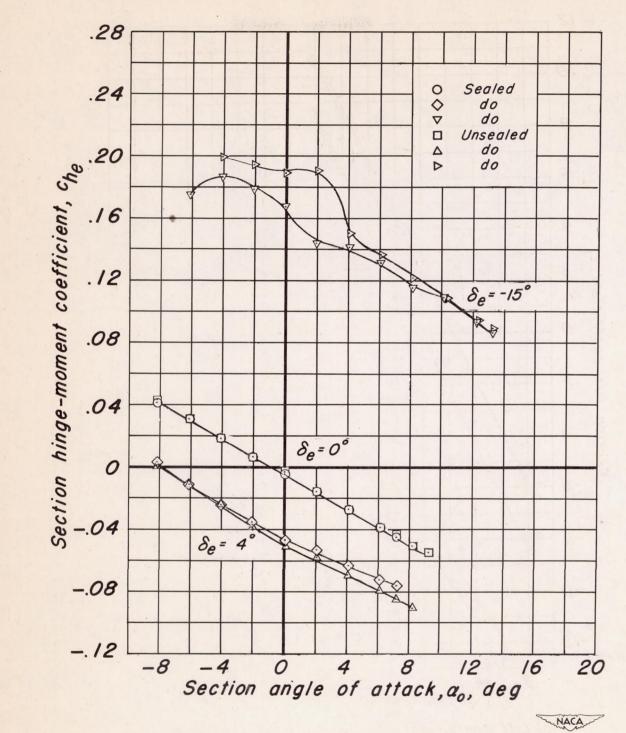


Figure 18.— Comparison of the section lift and hinge-moment coefficients of the NACA 64A010 airfoil with and without elevator seal. R, 4.0×10^6 .



(b) Hinge-moment coefficient.

Figure 18.-Concluded.

